ELSEVIER

Materials Science and Engineering A 489 (2008) 234–244

MATERIALS SCIENCE & ENGINEERING A

www.elsevier.com/locate/msea

Analytical modeling to calculate the hardness of ultra-fine WC–Co cemented carbides

Seung I. Cha [a], Kyong H. Lee [b], Ho J. Ryu [c], Soon H. Hong [b,*]

[a] *International Center for Young Scientists, National Institute for Materials Science 1-1, Namiki, Tsukuba 305-0044, Japan*

[b] *Department of Materials Science and Engineering, Korea Advanced Institute of Science and Technology, 373-1, Guseong-dong, Yuseong-gu, Daejeon 305-701, Republic of Korea*

[c] *DUPIC, Korea Atomic Energy Research Institute, 150 Deokjin-dong, Yuseong-gu, Daejeon 305-353, Republic of Korea*

Received 4 October 2007; received in revised form 10 December 2007; accepted 10 December 2007

Abstract

An analytical model to calculate the hardness of ultra-fine WC–10Co cemented carbides was investigated. The nanocrystalline WC–10Co powders were manufactured using a spray conversion process and sintered at 1375 °C in a vacuum. Varying amounts of TaC, Cr_3C_2, and VC were added to nanocrystalline WC–10Co cemented carbides as grain growth inhibitors. The hardness of WC–10Co cemented carbides increased with a decreasing WC grain size from 5 μm to 300 nm. An analytical model to calculate the hardness of WC–10Co cemented carbides was proposed under the assumption that the applied load is transferred from the WC to the Co binder phase. The analytically calculated hardness showed good agreement with the experimentally measured hardness of WC–10Co cemented carbides. In the proposed analytical model, the hardness of WC–10Co cemented carbides is similar to that predicted by the Hall–Petch relationship when the WC grain size is large. However, when the grain size is finer than a critical value, the predicted hardness of the WC–10Co cemented carbide becomes saturated.

Keywords: WC–Co; Cemented carbides; Ultra-fine; Hardness

1. Introduction

Cemented carbides, consisting of WC grains bound by a Co binder phase, have been used for cutting tools, rock drill tips, and other wear-resistant components during the last several decades. Recently, ultra-fine WC–Co cemented carbides have been developed using a thermochemical and thermomechanical process, called the spray conversion process, in order to improve the carbides' mechanical performance [1]. The WC particle size in powders fabricated using the spray conversion process can be reduced to approximately 100 nm. If the grain growth behavior is properly controlled during the sintering process, the WC grain size in sintered cemented carbides can be reduced to less than 400 nm [1–3].

Several results of the fracture toughness of ultra-fine WC–Co cemented carbides have been published [2–4]; however, little researches on the hardness of ultra-fine WC–Co cemented carbides, one of the most important indications used to evaluate the mechanical performance of cemented carbides, has been reported. The Hall–Petch relationship has been used to analyze the hardness of cemented carbides; however, the Hall–Petch relationship was derived theoretically for single-phase materials. Therefore, more theoretical studies are required to apply the Hall–Petch relationship to the hardness of cemented carbides, which consist of two phases including the WC phase and the Co binder phase. Moreover, even in monolithic materials, the hardness does not follow the Hall–Petch relationship if the grain size is finer than a critical value [5,6]. Therefore, more careful consideration regarding the hardness of ultra-fine cemented carbides is needed.

* Corresponding author. Tel.: +82 42 869 3327; fax: +82 42 869 3310.
E-mail address: shhong@kaist.ac.kr (S.H. Hong).

0921-5093/$ – see front matter © 2007 Elsevier B.V. All rights reserved.
doi:10.1016/j.msea.2007.12.036

In this study, the hardness of WC–Co cemented carbides is predicted by varying the WC grain size using an analytical model based on a load transfer theory. The estimated hardness was compared with the measured hardness of ultra-fine WC–Co cemented carbides fabricated using the spray conversion process.

2. Modeling for the hardness of WC–Co cemented carbides

2.1. Previous theories on the hardness of WC–Co cemented carbides

The first analysis for the deformation of WC–Co cemented carbides is based on the Orowan bowing of dislocation due to WC grains by considering the cemented carbides as dispersion-strengthened materials [7,8]. This analysis is proposed to predict the prediction of transverse rupture strength, which is considered to be related to the yielding or plastic deformation of WC–Co cemented carbides [7]. In this analysis, the yield strength, which is related to hardness, can be expressed as:

$$\sigma = \sigma_0 + \sqrt{k\frac{f^{2/3}}{d}}, \tag{1}$$

where k is the material constant, d is the WC grain size and σ_0 is the yield strength of the cemented carbides when there is no WC. Considering the microstructural factors, the hardness increases with an increasing WC volume fraction, f, and with a decreasing WC grain size, d. When the volume fraction of WC is fixed, Eq. (1) is a Hall–Petch relationship in which the yield strength is proportional to $1/\sqrt{d}$.

Lee and Gurland [9] suggested a model to evaluate the hardness of cemented carbides using a rule-of-mixtures and continuous volume concept. They considered WC–Co cemented carbides as composite materials, as follows:

$$H_C = CV_{WC}H_{WC} + (1 - CV_{WC})H_{Co}, \tag{2}$$

where C is the WC/WC contiguity, V_{WC} is the volume fraction of the WC phase in the WC–Co cemented carbides, and H_{WC} and H_{Co} are the hardness of WC phase and Co binder phase, respectively, which can be expressed as:

$$\begin{aligned} H_{WC} &= 1382 + \frac{23.1}{\sqrt{d}}\ (\mathrm{kg/mm^2}) \\ H_{Co} &= 304 + \frac{12.7}{\sqrt{\lambda}}\ (\mathrm{kg/mm^2}) \end{aligned}, \tag{3}$$

where d and λ are the WC grain size and Co mean free path, respectively, in units of μm. In Eqs. (2) and (3), the hardness of the WC–Co cemented carbides is represented as a Hall–Petch relationship between the WC grain size and Co mean free path. The relationship between the microstructural factors in the WC–Co cemented carbides can be expressed as in the following Eq. (4):

$$d = \lambda(1 - C)\frac{f}{1 - f}, \tag{4}$$

where f is the volume fraction of the WC in the WC–Co cemented carbides. For a fixed f and C, the simple equation for hardness can be obtained by substituting λ in Eq. (4) for those in Eqs. (2) and (3) as follows [10,11]:

$$H_C = H_0 + \frac{K}{\sqrt{d}}, \tag{5}$$

where H_0 and K are constants. Eq. (5) is also a Hall–Petch relationship of WC grain size. Therefore, even though WC–Co is not a single-phase material, the Hall–Petch relationship can be derived for hardness.

More microscopic considerations for the hardness of WC–Co cemented carbides were proposed recently by Nabarro et al. [12] based on the dislocation pile-up in the Co binder phase due to the WC grains. In this consideration, yielding occurs at the WC/WC interface due to the concentrated stress formed by the dislocation pile-up in the Co binder phase. Then, the hardness of the WC–Co cemented carbides can be predicted by following equation:

$$H_{WC/Co} = 4100\left[22.3\left(\frac{\lambda}{\sqrt{d}}\right)^{1/2} + 1\right]^{-1} - 130. \tag{6}$$

In Eq. (6), the hardness of the WC–Co cemented carbides does not obey the Hall–Petch relationship. However, by applying the microstructural relationship in Eq. (4) to the above relationship, the hardness increases with a decreasing WC grain size. The above relationships between the WC grain size and the hardness of the WC–Co cemented carbides are supported by experimental data for the hardness of conventional carbides [10–12]. However, the above relationships predict that the hardness of cemented carbides increases continuously to infinity while decreasing the WC grain size to zero. This can be problematic when the hardness of ultra-fine

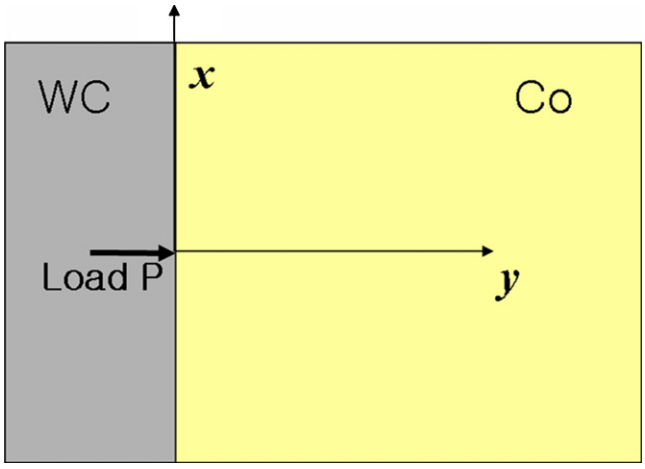

Fig. 1. Schematic unit cell showing the *x*-, *y*-axes used to calculate the stress transferred from a single WC–Co interface to the Co binder phase in WC–Co cemented carbides.

or nanocrystalline WC–Co cemented carbides is considered. In order to overcome this problem, Engqvist et al. [13] proposed an empirical relationship by introducing a new constant within the Hall–Petch relationship that considers the thickness effect of the Co binder phase, so that the hardness does not increase infinitely when the WC grain size becomes zero. This is expressed as follows:

$$H_{\mathrm{WC/Co}} = \left[693 + \frac{2680}{\sqrt{2.1+d}} - 825\right] \mathrm{e}^{-\lambda/k} + 825, \tag{7}$$

where λ is the Co mean free path, d is the WC grain size, and k is the hardening range factor. This relationship predicts a finite hardness value of the WC–Co cemented carbides when the WC grain size decreases to zero. However, it does not contain a theoretical analysis, but rather an empirical relationship.

2.2. Analytical modeling for the hardness of ultra-fine WC–Co cemented carbides

Although there are some models that predict the hardness of WC–Co cemented carbides [7–13], they are inadequate to predict it when the WC grain size decreases to sub-micrometer sizes. Therefore, a new theoretical approach is needed to analyze the hardness of ultra-fine WC–Co cemented carbides.

The WC–Co cemented carbides consist of two phases: a WC phase and a Co binder phase. Generally, the WC phase shows a larger volume fraction, a higher elastic modulus, and a higher yield strength than the Co binder phase. Therefore, it can be assumed that the bulk of the external load applied to WC–10Co cemented carbides is supported by the WC skeletons due to their high volume fraction and strength. Then, the stress field inside the Co binder phase is induced by the load transfer from the WC skeleton to the WC–Co interface. In this case, despite the higher applied load in the WC skeleton, yielding occurs in the Co binder phase near the WC–Co interface because the yield strength of Co is much lower than that of the WC skeleton. Therefore, for the yielding of the WC–Co cemented carbide, the stress distribution within the Co binder phase should be considered first.

In order to calculate the stress field in the Co binder phase, which is induced by the load transfer from the WC to the WC–Co interface, a simple boundary model was considered as shown in Fig. 1. Then, the stress field within the Co binder phase can be calculated considering the boundary conditions, in which $P=(P_x, P_y)$ is applied to the Co binder phase at $y=0$ in Fig. 1. With the above assumptions, the elastic deformation of the Co binder phase can be calculated using the following equilibrium equation if the Co phase is isotropic:

$$2(1-\nu)\nabla(\nabla\cdot u) - (1-2\nu)\nabla\times(\nabla\times u) = 0, \tag{8}$$

where u is the displacement vector. If the load is transferred from the WC–Co interface only, then the stress decreases to zero at an infinite distance from the WC–Co interface. Based on the above situation, the analytical solution of Eq. (8) is as follows when the load at the WC–Co interface $F=(F_x, F_y)$ is concentrated at $x=x'$ such as $F=P\delta(x')$ where $\delta(x)$ is a Delta function [14] (see Appendix A):

$$\begin{aligned} u_x &= \frac{1+\nu}{2\pi E}\left[\left\{\frac{xy}{r^3} - \frac{(1-2\nu)x}{r(r+y)}\right\}F_y + \left\{\frac{2(1-\nu)r+y}{r(r+y)} + \frac{(2r(\nu r+y)+y^2)x^2}{r^3(r+y)^2}\right\}F_x\right] \\ u_y &= \frac{1+\nu}{2\pi E}\left[\left\{\frac{y^2}{r^3} + \frac{2(1-\nu)}{r}\right\}F_y + \left\{\frac{1-2\nu}{r(r+y)} + \frac{y}{r^3}\right\}xF_x\right] \end{aligned}. \tag{9}$$

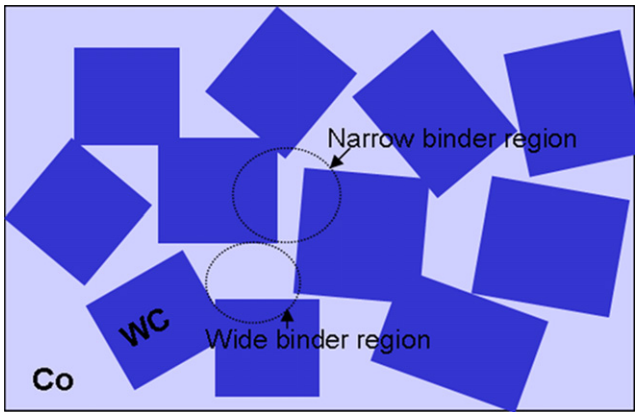

Fig. 2. Schematic microstructure of sintered WC–10Co cemented carbides.

If the force at the boundary is applied in a normal direction to the interface, $F_x = 0$, the solution becomes simpler, as in Eq. (10):

$$\begin{aligned} u_x &= \frac{1+\nu}{2\pi E}\left[\left\{\frac{xy}{r^3} - \frac{(1-2\nu)x}{r(r+y)}\right\}F_y\right] \\ u_y &= \frac{1+\nu}{2\pi E}\left[\left\{\frac{y^2}{r^3} + \frac{2(1-\nu)}{r}\right\}F_y\right] \end{aligned} . \tag{10}$$

For an arbitrary load at the WC–Co interface, the solution can be obtained using Green function theory as follows:

$$\begin{aligned} u_i &= \int G_{ik}(x-x', y)P(x', y)\,\mathrm{d}x' \\ u_1 &= \frac{1+\nu}{2\pi E}\int\left[\left\{\frac{(x-x')y}{\sqrt{(x-x')^2+y^2}^3} - \frac{(1-2\nu)x}{\sqrt{(x-x')^2+y^2}\left(\sqrt{(x-x')^2+y^2}+y\right)}\right\}P(x', y)\right]\mathrm{d}x' \\ u_2 &= \frac{1+\nu}{2\pi E}\int\left[\left\{\frac{y^2}{\sqrt{(x-x')^2+y^2}^3} + \frac{2(1-\nu)}{\sqrt{(x-x')^2+y^2}}\right\}P(x', y)\right]\mathrm{d}x' \end{aligned} , \tag{11}$$

where G is the Green function for the load, i.e. the solution for the concentrated force F.

Considering the microstructure of the WC–Co cemented carbides, two types of Co binder phase exist: one is a region with a narrow thickness between two neighboring WC grains (narrow binder region) and the other is a region with a wider thickness surrounded by several WC grains (wide binder region), as shown in Fig. 2. In the narrow binder region, the stress becomes high due to the low spacing between the interfaces, while the stress in wider binder region is low. Therefore, it is expected that the load transferred from the WC to the Co binder has a stress gradient between the narrow binder and wide binder regions. In order to calculate the stress distribution within the Co binder phase, the microstructure of the WC–10Co cemented carbides was simplified and modeled as shown in Fig. 3, in which the narrow binder region has a width of λ and a WC grain size of $2d$. Based on the model in Fig. 3, the stress states at the narrow binder and wide binder regions are analyzed. When the direction of the load transferred from the WC to the Co binder phase is normal to the interface, from the relationship in Eq. (10), the shear stress from concentrated force F at (0, 0) in Fig. 3 can be obtained as follows:

$$\tau = G\frac{1}{2}\left(\frac{\partial u_2}{\partial x} + \frac{\partial u_1}{\partial y}\right). \tag{12}$$

$$\tau = \frac{F}{8\pi}\frac{x}{r}\left[\frac{1}{r^2}\left\{\frac{(1-2\nu)y}{r+y} + (3-2\nu)\right\} + \frac{(1-2\nu)((y/r)+1)}{(r+y)^2} - 6\frac{y^2}{r^4}\right] = \Theta F,$$

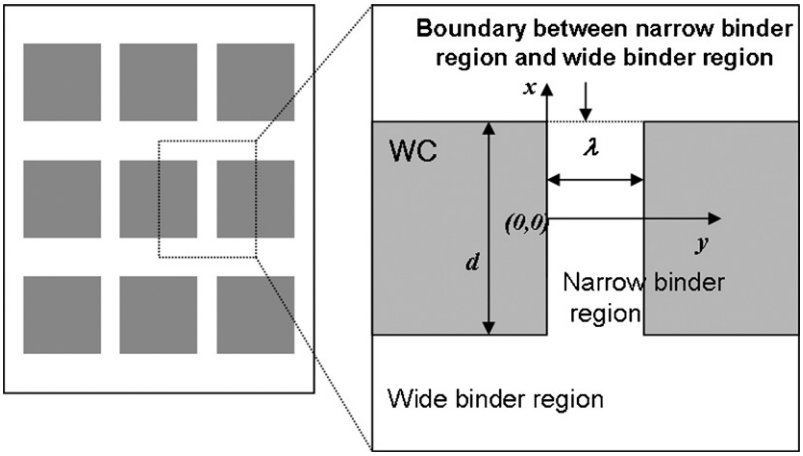

Fig. 3. Unit cell model for the microstructure of WC–Co cemented carbides showing the narrow binder and wide binder regions used to calculate the shear stress on the binder phase.

where x and y are the coordinates indicated in Fig. 3, r is $\sqrt{x^2+y^2}$, and ν is Poisson's ratio of the Co binder phase. If a constant force F is applied to the WC–Co interface, the shear stress at the Co binder phase can be obtained as follows:

$$\tau_{\mathrm{Co}} = \int_{-d/2}^{d/2} \Theta(x-x', y) F(x')\,\mathrm{d}x'$$
$$\tau_{\mathrm{Co}} = \frac{F}{4\pi}\left[\frac{y^2(1-2\nu)+2(x-(d/2))^2(1-\nu)}{\sqrt{(x-(d/2))^2+y^2}^3} - \frac{y^2(1-2\nu)+2(x+(d/2))^2(1-\nu)}{\sqrt{(x+(d/2))^2+y^2}^3}\right]. \tag{13}$$

The shear stress distribution expressed in Eq. (13) is plotted in Fig. 4(a). The shear stress near the boundary between the wide binder and narrow binder regions is higher than that of other places in the Co binder phase, as shown in Fig. 4(a). Therefore, it is concluded that the yielding of the Co binder phase occurs near the boundary between the wide binder region and the narrow binder region, as illustrated in Fig. 4(b). The shear stress on the boundary between the wide binder and narrow binder regions can be obtained as follows:

$$\tau_{\mathrm{Co}} = \frac{F}{4\pi}\left[\frac{y^2(1-2\nu)+2d^2(1-\nu)}{\sqrt{d^2+y^2}^3} - \frac{(1-2\nu)}{y}\right] = \Psi F. \tag{14}$$

Therefore, the average shear stress which is transferred from the WC to the boundary between the wide binder region and the narrow binder region can be obtained by integrating Eq. (14) with respect to y in the range between 0 and λ and divided by λ, as shown in Eq. (15).

$$\bar{\tau}_{\mathrm{Co}} = \frac{1}{\lambda}\int_0^{\lambda} \Psi F\,\mathrm{d}y$$
$$\bar{\tau}_{\mathrm{Co}} = \frac{1}{2\pi\lambda}\left[-\frac{\lambda}{\sqrt{\lambda^2+d^2}} - (1-2\nu)\ln\left(1+\frac{\sqrt{d^2+\lambda^2}}{\lambda}\right)\right]F. \tag{15}$$

The yielding of the cemented carbides occurs when the average shear stress reaches a critical value. Therefore, the yielding condition of the cemented carbides can be obtained as follows:

$$|\bar{\tau}_{\mathrm{Co}}| = \frac{T}{2\pi}\left[\frac{\lambda}{\sqrt{\lambda^2+d^2}} + (1-2\nu)\ln\left(1+\frac{\sqrt{\lambda^2+d^2}}{\lambda}\right)\right] = \tau_{\mathrm{c}}, \tag{16}$$

where $T=|-F/\lambda|$ indicates the external stress required in order to yield the cemented carbides. Then, the hardness of WC–Co cemented carbides is derived as follows:

$$H = \frac{2\pi H_{0,\mathrm{Co}}}{\left(\lambda/\sqrt{\lambda^2+d^2}\right)+(1-2\nu)\,\ln\left(1+\left(\sqrt{\lambda^2+d^2}/\lambda\right)\right)}. \tag{17}$$

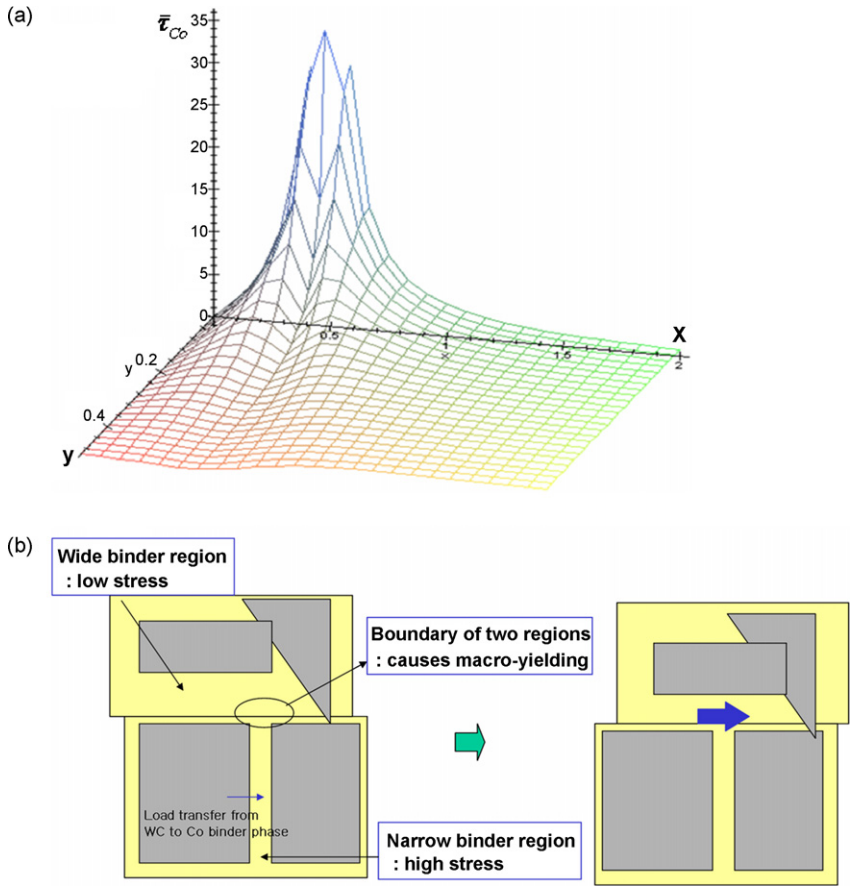

Fig. 4. (a) The distribution of shear stress near the boundary between the narrow binder region and the wide binder region WC–Co cemented carbide when the WC grain size is 1 μm, and (b) the schematic illustration of the yielding criteria in the WC–Co cemented carbides.

In Fig. 5, the hardness of the cemented carbide normalized by $H_{0,Co}$ is plotted with the grain size of WC, $2d$. In Fig. 5, the hardness of the cemented carbides becomes closer to the Hall–Petch relationship with a decreasing λ to zero. This indicates that when λ reaches zero, the microstructures in the model become similar to those of single-phase materials. Also, when the grain size of the WC increases, the hardness values become similar to those predicted by the Hall–Petch relationship.

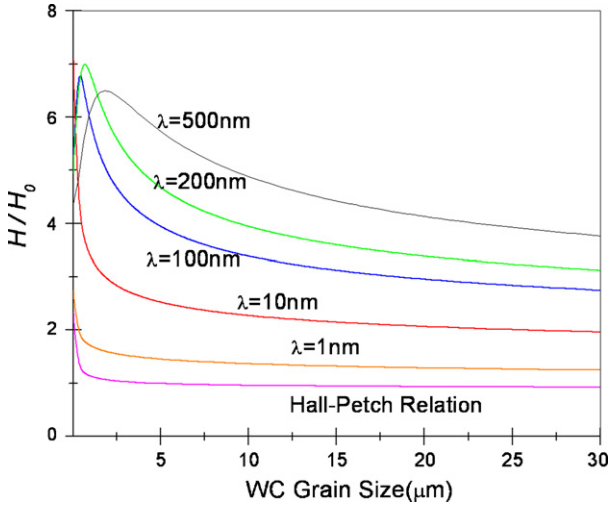

Fig. 5. The ratio of the hardness (H) of cemented carbides to the hardness of the Co binder phase (H_0) in WC–Co cemented carbides with varying WC grain sizes with various values of λ.

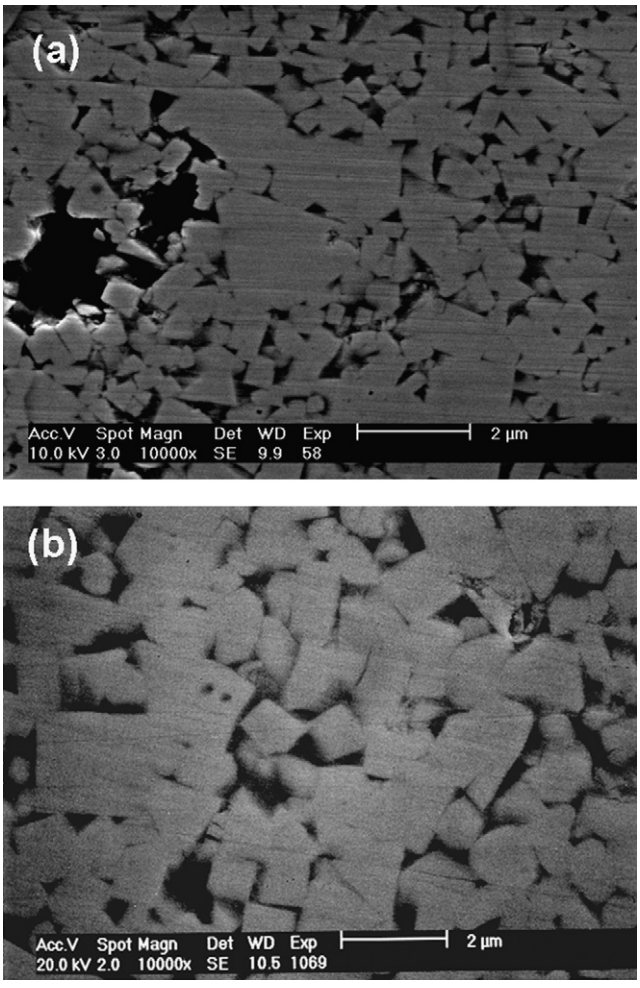

Fig. 6. SEM micrographs of ultra-fine and conventional WC–10Co cemented carbides sintered at 1375 °C for 1 h. (a) Ultra-fine WC–10Co and (b) conventional WC–10Co.

3. Experimental procedures

The precursor WC–10Co powders were prepared using a spray conversion process from a solution containing ammonium meta-tungstate (AMT) and $Co(NO_3)_2$, and were followed by oxidation, reduction, and carbonization processes. The average size of the WC particles in the precursor powders was 100 nm and the WC nanocrystalline particles were homogeneously mixed with the Co phase [3,4]. The precursor WC–10Co powders were wet ball-milled in *n*-hexane for homogeneous mixing with paraffin for 24 h. The ball-milled powders were dried in an oven for 24 h at 80 °C and were compacted under a pressure of 20 MPa at room temperature. The compacted powders were consolidated by liquid phase sintering at 1375 °C for 1–5 h under a pressure of 1 mTorr. The microstructure of the sintered WC–Co cemented carbides was analyzed using a scanning electron microscope (SEM). The hardness of the sintered WC–10Co cemented carbides was measured by Vicker's hardness tester under a constant load of 9.8 N. The microstructure of the ultra-fine and conventional WC–10Co cemented carbides could be controlled by the addition of a grain growth inhibitor, as shown in Fig. 6. The grain size of the ultra-fine WC–10Co–0.7TaC/VC could be reduced to 300 nm, while the grain size of ultra-fine WC–10Co was 700 nm when sintered at 1375 °C for 1 h. The Vicker's hardness of ultra-fine and conventional WC–10Co with various WC grain sizes is shown in Fig. 7. In this figure, the hardness of the WC–10Co cemented carbides increases with a decreasing WC grain size ranging from 300 nm to 5 μm.

4. Results and discussion

In the Hall–Petch relationship, the hardness of cemented carbides can be predicted by fitting the hardness data against $d^{-1/2}$ and by determining the related constants H_0 and k. Also, the hardness of cemented carbides can be predicted with the proposed model by fitting the measured data and by determining $H_{0,Co}$ and λ as in the following equation. The relationship between the hardness of

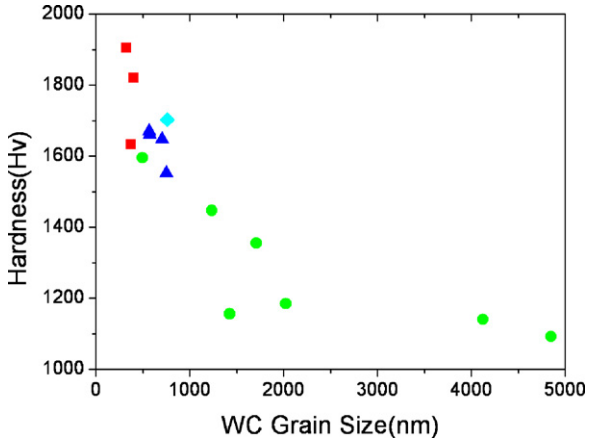

Fig. 7. The variation of hardness of the WC–10Co cemented carbides with varying WC grain sizes.

WC–Co cemented carbides and WC grain size based on the proposed model is obtained by:

$$H = \frac{2\pi \times 291.7\,(\mathrm{H_v})}{\left(0.06/\sqrt{0.06^2 + d\,(\mu\mathrm{m})^2}\right) + (1-2\nu)\,\ln\left(1 + \left(\sqrt{0.06^2 + d\,(\mu\mathrm{m})^2}/0.06\right)\right)}. \tag{18}$$

Comparing the above equation to Eq. (17), $H_{0,\mathrm{Co}}$, which indicates the hardness of the Co binder phase, was determined to be 291.7 $\mathrm{H_v}$. This value is very similar to the hardness value of pure Co, which is known to be 150–250 $\mathrm{H_v}$. [15] In Fig. 8, both the Hall–Petch relationship and the proposed model can predict well the measured hardness values of the WC–Co cemented carbides when the WC grain size is larger than 0.7 μm. However, only the proposed model can predict the measured hardness when the WC grain size is below 0.7 μm.

In the proposed model, the hardness of the cemented carbides decreases with a decreasing WC grain size below the critical value. However, the critical WC grain size, below which the hardness of the cemented carbides decreases, varies with λ, the width of the narrow binder region, as shown in Fig. 5. If the WC grain size is sufficiently large, constant λ values exist below which the Co binder phase cannot deform. However, when the WC grain size is very small, the Co mean free path decreases and becomes smaller than the λ fitted in Fig. 8, which is 0.06 μm. When the Co mean free path becomes close to λ, there is almost no difference in the stress transferred from the WC–Co interface in the narrow binder region and the wide binder region. Therefore, there is no stress gradient between the narrow binder region and the wide binder region. In this case, λ is considered as the mean free path of the Co binder phase which decreases linearly with a decreasing the WC grain size because there are no differences between the narrow binder region and the wide binder region in deformation. Therefore, if the WC grain size is small enough that the Co mean free path is close to or less than λ, the relationship exists as follows:

$$\lambda = \alpha d, \tag{19}$$

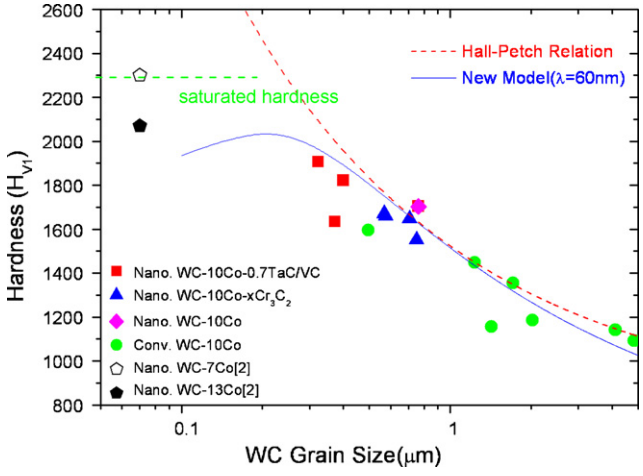

Fig. 8. The variation of the hardness of WC–10Co cemented carbides with varying WC grain sizes. The dotted lines were fitted by the Hall–Petch relationship, and the solid lines were fitted by the proposed model.

where α is constant. In this case, the hardness of the WC–Co cemented carbides can be obtained as in the following relation:

$$H = \frac{2\pi H_{0,\mathrm{Co}}}{\left(1/\sqrt{1+\alpha^2}\right) + (1-2\nu)\,\ln\left(1+\sqrt{1+\alpha^2}\right)}. \tag{20}$$

α can be calculated by finding λ for each d so that no stress gradient exists at $x = d/2$ in Fig. 3. Therefore, as the WC grain size decreases, the hardness of the WC–Co cemented carbide becomes saturated to the critical value expressed by Eq. (20). The calculated value of α is 3. Therefore, the hardness of the WC–Co cemented carbides saturates to a value of 2300 kg/mm^2 when the WC grain size becomes zero. If the proposed model is reasonable, it must be noted that the predicted hardness of the WC–Co cemented carbide is not infinite, but saturated to 2300 kg/mm^2 when the WC grain size decreases to zero. In Fig. 8, the hardness of the WC–7Co and WC–13Co cemented carbides with a grain size of 70 nm is presented [2]. It is notable that the hardness of the nanocrystalline WC–7Co cemented carbides does not increase according to the Hall–Petch relationship, which predicts a much higher hardness than the experimentally measured hardness shown in Fig. 8, instead, it is saturated to the value predicted by the proposed model. Therefore, the hardness of the WC–Co cemented carbides follows the proposed model: it increases with a decreasing WC grain size and saturates to a critical value when the WC grain size is finer than a critical value.

5. Conclusion

The hardness of ultra-fine WC–10Co cemented carbides increases as the WC grain size decreases from 300 nm to 5 μm.In order to predict the hardness of nanocrystalline WC–Co cemented carbides, a new analytical model is proposed under the assumption that the load is transferred from the WC to the Co in the WC–Co cemented carbides and a stress gradient exists in the Co binder phase of the WC–Co cemented carbides. In this model, the Co binder phase is divided into a narrow binder region with a high stress and a wide binder region. The yielding was assumed to occur when the shear stress at the boundary between the two binder regions is above the critical shear stress of Co.Using the proposed model, a new relationship between hardness and WC grain size was obtained, as follows:

$$H = \frac{2\pi \times 291.7}{\left(0.06/\sqrt{0.06^2+d^2}\right) + (1-2\nu)\ln\left(1+\left(\sqrt{0.06^2+d^2}/0.06\right)\right)}$$

In this relationship, when the grain size is large, the predicted value is similar to the values predicted by the Hall–Petch relationship. However, if the grain size is finer than a critical value, the hardness does not increase any further with a decreasing WC grain size.The experimentally measured hardness of the WC–Co cemented carbides was well predicted using the proposed model. The proposed model can predict the hardness of the WC–Co cemented carbides with WC grain sizes below 1 μm, which cannot be predicted by the Hall–Petch relationship.

Appendix A

The solution of the following equations is well known for specific boundary conditions in the published literature [14].

$$2(1-\nu)\nabla(\nabla\cdot u) - (1-2\nu)\nabla\times(\nabla\times u) = 0 \tag{A.1}$$

It is assumed that the solution of Eq. (A.1) is a summation of two harmonic functions because u is harmonic in an isotropic body. Then, u can be expressed as follows:

$$u = f + \nabla\phi, \tag{A.2}$$

where ϕ is a scalar function. Eq. (A.1) can be expressed as a function of f and ϕ as in Eq. (A.3):

$$2(1-\nu)\nabla^2\phi = -\nabla\cdot f. \tag{A.3}$$

It can be assumed that the vector f is a derivative of the scalar function g as follows:

$$f = \left(\frac{\partial g_x}{\partial y}, g_y\right). \tag{A.4}$$

Then, Eq. (A.3) can be expressed as a function of scalar values as in Eq. (A.5):

$$2(1-\nu)\nabla^2\phi = -\frac{\partial}{\partial y}\left(\frac{\partial g_x}{\partial x} + g_y\right). \tag{A.5}$$

To solve Eq. (A.5), the auxiliary function Ψ is introduced, which satisfies Laplace's equation. Then, the solution is as follows:

$$\phi = -\frac{y}{4(1-\nu)}\left(\frac{\partial g_x}{\partial x} + g_y\right) + \Psi. \tag{A.6}$$

Then, the differential equation of Eq. (A.1) is reduced to Eq. (A.6) as a function of scalar variables only. In the assumption, the boundary is $y=0$ and a pressure P is applied; then Eq. (A.6) is reduced to:

$$\begin{aligned} &\left.\frac{\partial^2 g_x}{\partial y^2}\right|_{y=0} + \left[\frac{\partial}{\partial x}\left\{\frac{1-2\nu}{2(1-\nu)}g_y - \frac{1}{2(1-\nu)}\frac{\partial g_x}{\partial x} + 2\frac{\partial \Psi}{\partial y}\right\}\right]_{y=0} = -\frac{2(1+\nu)}{E}P_x \\ &\left[\frac{\partial}{\partial y}\left\{g_y - \frac{\partial g_x}{\partial x} + 2\frac{\partial \Psi}{\partial y}\right\}\right]_{y=0} = -\frac{2(1+\nu)}{E}P_y \end{aligned}. \tag{A.7}$$

Eq. (A.7) is two known relations; however, there are three unknown variables. Therefore, one more relation between the variables needs to be derived. If the variables are chosen as in Eq. (A.8), then the solution can be obtained in simpler form:

$$\left[\frac{\partial}{\partial x}\left\{\frac{1-2\nu}{2(1-\nu)}g_y - \frac{1}{2(1-\nu)}\frac{\partial g_x}{\partial x} + 2\frac{\partial \Psi}{\partial y}\right\}\right] = 0. \tag{A.8}$$

Then, the solutions are:

$$\begin{aligned} &\left[\frac{\partial}{\partial x}\left\{\frac{1-2\nu}{2(1-\nu)}g_y - \frac{1}{2(1-\nu)}\frac{\partial g_x}{\partial x} + 2\frac{\partial \Psi}{\partial y}\right\}\right] = 0 \\ &\left.\frac{\partial^2 g_x}{\partial y^2}\right|_{y=0} = -\frac{2(1+\nu)}{E}P_x \\ &\left[\frac{\partial}{\partial y}\left\{g_y - \frac{\partial g_x}{\partial x} + 2\frac{\partial \Psi}{\partial y}\right\}\right]_{y=0} = -\frac{2(1+\nu)}{E}P_y \end{aligned}. \tag{A.9}$$

If the boundary load is given by a Delta function, i.e. the concentrated loading, Eq. (A.10) can be derived:

$$P = F\delta(x). \tag{A.10}$$

Then, for P, it is zero without x' and a harmonic function. If a harmonic function is zero at infinity, then the potential theory is applied as follows:

$$\begin{aligned} &f(x,y) = -\frac{1}{2\pi}\int \left.\frac{\partial f(x'y)}{\partial y}\right|_{y=0}\frac{\mathrm{d}x'}{r} \\ &r = \sqrt{(x-x')^2 + y^2} \end{aligned}. \tag{A.11}$$

Therefore, the solutions in Eq. (A.9) should satisfy the potential theory. Then, the following solution is obtained:

$$\begin{aligned} &\left[\frac{\partial}{\partial y}\left\{g_y - \frac{\partial g_x}{\partial x} + 2\frac{\partial \Psi}{\partial y}\right\}\right] = -\frac{(1+\nu)}{\pi E}\int \frac{P_y}{r}\,\mathrm{d}x = \frac{1+\nu}{\pi E}\frac{Fy}{r} \\ &\frac{\partial^2 g_x}{\partial y^2} = -\frac{1+\nu}{\pi E}\frac{F_x}{r} \end{aligned}. \tag{A.12}$$

u can be calculated by substituting Eq. (A.12) into Eq. (A.9) as follows:

$$\begin{aligned} u_x &= \frac{1+\nu}{2\pi E}\left[\left\{\frac{xy}{r^3} - \frac{(1-2\nu)x}{r(r+y)}\right\}F_y + \left\{\frac{2(1-\nu)r+y}{r(r+y)} + \frac{(2r(\nu r+y)+y^2)x^2}{r^3(r+y)^2}\right\}P_x\right] \\ u_y &= \frac{1+\nu}{2\pi E}\left[\left\{\frac{y^2}{r^3} + \frac{2(1-\nu)}{r}\right\}F_y + \left\{\frac{1-2\nu}{r(r+y)} + \frac{y}{r^3}\right\}xP_y\right] \end{aligned}. \tag{A.13}$$

References

[1] B.K. Kim, G.H. Ha, D.W. Lee, J. Mater. Process. Technol. 63 (1997) 317.
[2] K. Jia, T.E. Fischer, B. Gallois, Nanostruct. Mater. 10 (5) (1998) 875.
[3] S.I. Cha, S.H. Hong, G.H. Ha, B.K. Kim, Scripta Mater. 44 (8/9) (2001) 1535.
[4] S.I. Cha, S.H. Hong, G.H. Ha, B.K. Kim, Int. J. Refract. Met. Hard Mater. 19 (2001) 397.
[5] H. Gleiter, Prog. Mater. Sci. 33 (1989) 223.
[6] C. Suryanarayana, C.C. Koch, Hyperfine Interact. 130 (2000) 5.

[7] J. Gurlnd, Trans. Metall. Soc. AIME 227 (1963) 1146.
[8] H. Doi, Y. Fujiwara, K. Miyake, Trans. Metall. Soc. AIME 245 (1969) 1457.
[9] H.C. Lee, J. Gurland, Mater. Sci. Eng. 33 (1978) 125.
[10] Y.V. Milman, S. Luyckx, I. Northrop, Int. J. Refract. Hard Mater. 17 (1999) 39.
[11] Y.V. Milman, S. Chugunova, V. Goncharyck, S. Luyckx, I. Northrop, Int. J. Refract. Hard Mater. 15 (1997) 97.
[12] F.R.N. Nabarro, L. Makhele, S. Luyckx, Presentations at Seventh International Conference on the Science of Hard Materials, Ixtapa, Mexico March 5–9, 2001.
[13] H. Engqvist, S. Jacobson, N. Axén, Wear 252 (2002) 384.
[14] L.D. Landau, E.M. Lifshitz, Theory of Elasticity, Butterworth-Heinenann Ltd., Oxford, 1986, p. 22.
[15] W. Betteridge, Cobalt and Its Alloys, Ellis Horwood Limited and John Wiley and Sons, 1982.